Bioorganic Chemistry 97 (2020) 103703

Contents lists available at ScienceDirect

Bioorganic Chemistry

journal homepage: www.elsevier.com/locate/bioorg

N-Metallocenoylsphingosines as targeted ceramidase inhibitors: Syntheses and antitumoral effects

Matthias Rothemund[a,1], Alexander Bär[a,1], Felix Klatt[b], Sascha Weidler[c], Leonhard Köhler[a], Carlo Unverzagt[c], Claus-D. Kuhn[b], Rainer Schobert[a,*]

[a] Department of Chemistry, University Bayreuth, Universitaetsstrasse 30, 95440 Bayreuth, Germany
[b] Gene Regulation by Non-Coding RNA, Elite Network of Bavaria and University of Bayreuth, Universitaetsstr. 30, 95447 Bayreuth, Germany
[c] Bioorganic Chemistry, University of Bayreuth, Universitaetsstr. 30, 95447 Bayreuth, Germany

ARTICLE INFO

Keywords:
Ceramidase inhibitors
Anticancer agents
Colocalization
Organometallic drugs
Sphingolipids

ABSTRACT

Three *N*-metallocenoylsphingosines with variance in the central metal (Fe, Co, Ru), the charge (neutral or cationic), and the arene ligands (Cp_2, Cp*Ph) were synthesized from serine and metallocene carboxylic acids as substrate-analogous inhibitors of human acid ceramidase (AC). Their inhibitory potential was examined using the recombinant full length ASAH1 enzyme, expressed and secreted from High Five insect cells, and the fluorescent substrate Rbm14-12. All complexes inhibited AC, most strongly so ruthenium(II) complex **13a**. Some antitumoral effects of the complexes, such as the interference with the microtubular and F-actin cytoskeleton of cancer cells, were correlated to their AC-inhibition, whereas others, e.g. their cytotoxicity and their induction of caspase-3/-7 activity in cancer cells, were not. All complexes accumulated preferentially in the lysosomes of cancer cells like their target AC, arrested the cells in G1 phase of the cell cycle, and displayed cytotoxicity with mostly single-digit micromolar IC_{50} values while inducing cancer cell apoptosis.

1. Introduction

The sphingolipid rheostat is a delicately balanced network of sphingosine derivatives and pertinent enzymes, regulating growth, differentiation, motility, survival and apoptosis of endothelial and cancer cells [1–4]. Key players of this rheostat are the cell death promoting ceramides (**1**, cer) and sphingosine (**2a**, sph), as well as sphingosine-1-phosphate (**3**, s1p) which promotes cell survival and proliferation (Fig. 1) [5–8]. Increased levels of cer and sph are associated with greater permeability of lysosomal and mitochondrial membranes, and thus with an activation of the lysosomal and the intrinsic apoptotic pathway [9–11]. Both metabolites were reported to impair cell cycle progression. Imbalancing the rheostat led to Golgi fragmentation and loss of cell-cell contacts, and eventually to anoikis and cell starvation [12,13]. The anti-apoptotic s1p can be generated only by conversion of cer to sph by ceramidases and a subsequent phosphorylation of sph by sphingosine kinases (SK) [14,15]. In human cells three types of ceramidases are known, called alkaline, neutral and acid ceramidase according to their pH optimum [1,2]. Due to its role in Farber's disease, a deficiency in lysosomal *N*-acylsphingosine-amidohydrolase activity, acid ceramidase (AC) probably is the most thoroughly investigated and most important ceramidase [16]. Ceramidases are often upregulated in cancer cells, resulting in an increase of s1p and consequently in higher survival rates and sustained cell proliferation [17–20]. Thus, the cer/s1p rheostat was recognized as a promising target for chemotherapeutic intervention in the treatment of cancer [6]. The inhibition of ceramidases is expected to lead to an accumulation of pro-apoptotic cer and to a depletion of anti-apoptotic s1p.

Early ceramidase inhibitors were structurally modelled on the natural ceramides, yet showed low activities and poor selectivities in *in vitro* assays [21–24]. Only a few derivatives showed a significant activity, e.g. analogues of *N*-oleoylethanolamine (NOE) and the ceramide analogue (1*S*,2*R*)-D-*erythro*-2-(*N*-myristoylamino)-1-phenyl-1-propanol (D-*e*-MAPP), whose antitumoral and ceramidase inhibitory effects were

Abbreviations: AC, acid ceramidase; ASAH1, *N*-acylsphingosine amidohydrolase 1; cer, ceramide; cpm, cells per mL; DIPEA, diisopropylethylamide; DMF, dimethylformamide; HBTU, (2-(1H-benzotriazol-1-yl)-1,1,3,3-tetramethyluronium hexafluorophosphate); JACoP, Just another colocalization plugin; LICQ, Li's Intensity Correlation Quotient; MTT, 3-(4,5-dimethylthiazol-2-yl)-2,5-diphenyltetrazolium bromide; NBT, nitroblue tetrazolium; PC, Pearson correlation coefficient; P-gp1, p-glycoprotein 1; sph, sphingosine; SK, sphingosine kinase; s1p, sphingosine-1-phosphate; vbl, vinblastine; vpm, verapamil

* Corresponding author.
E-mail address: Rainer.Schobert@uni-bayreuth.de (R. Schobert).
[1] These authors contributed equally to this work.

https://doi.org/10.1016/j.bioorg.2020.103703
Received 30 October 2019; Received in revised form 22 February 2020; Accepted 24 February 2020
Available online 25 February 2020

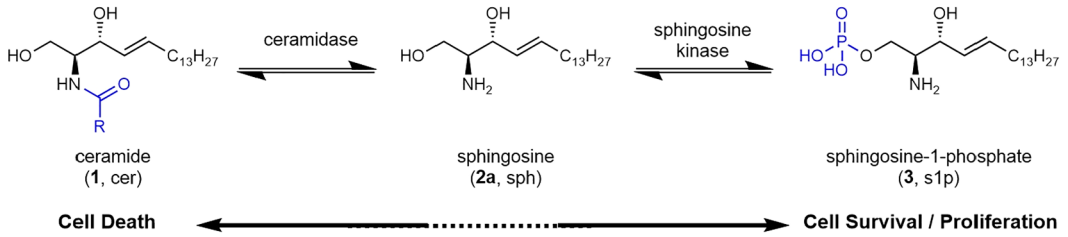

Fig. 1. Ceramide/sphingosine-1-phosphate rheostat: sphingosine-1-phosphate (**3**, s1p), promoting cell survival and proliferation, can be synthesized via hydrolyzation of cell death promoting ceramides (**1**, cer) by ceramidase to give sphingosine (**2a**, sph) and its downstream phosphorylation by sphingosine kinases (SK).

studied in detail [21,25,26]. More potent inhibitors, structurally unrelated to ceramide, were later identified by Draper et al. (e.g. ceranib-2) [27], Realini et al. (carmofur) [28] and others [21]. A major problem with developing new ceramidase inhibitors is the low comparability of literature data. Multiple methods for determining the efficacy of ceramidase inhibitors are in use, that differ in the conditions of the cellular assays, the purity of the enzymes, and the nature of the reporter substrates. More often than not, potential inhibitors were tested not on purified enzymes but on crude cell extracts of unknown enzyme concentration.

Following our successful strategy of covalently combining natural metabolites with bioactive metal complex fragments and metallocenes in particular [29], we developed new sphingosine–metallocene conjugates and investigated their antitumoral modes of action, as well as their AC-inhibitory activity on a purified human ceramidase enzyme.

2. Results and discussion

2.1. Chemistry

A series of novel organometallic AC-inhibitor candidates was prepared by *N*-acylation of sph (**2a**) and alkyne-labeled sph (**2b**) with different metallocene carboxylic acids. The two sphingoid bases **2** were synthesized from doubly protected serine ester **4** which was treated with excess lithium dimethyl methylphosphonate to be converted to the β-ketophosphonate **5** in excellent yield (Scheme 1). Its HWE reactions with tetradecanal and tetradec-13-ynal using NEt_3 as a base in the presence of anhydrous LiCl afforded the corresponding 3-ketosphingosines **6a** and **6b** [30]. The diastereoselective reduction of the enones was achieved using $LiAlH(OtBu)_3$ in analogy to a literature protocol [31]. Gratifyingly, only the desired *anti*-configured alcohols **7** were obtained in 75% and 77% yield, respectively. Their deprotection with TFA afforded the free sphingoid bases **2** in total yields of 67% and 64% over four steps. The sphingoid bases **2** were then linked to carboxyferrocene (**8**), carboxycobaltocenium hexafluorophosphate (**9**) and $[(\eta^5\text{-Cp}^*)(\eta^6\text{-}C_6H_5CO_2H)Ru]PF_6$ (**10**) using HBTU as a coupling reagent in the presence of excess DIPEA (Scheme 2). Purification by column chromatography over silica gel (for **11** and **13**), or precipitation with $NaBPh_4$ in MeOH (for **12**) afforded the corresponding amides **11**–**13** in

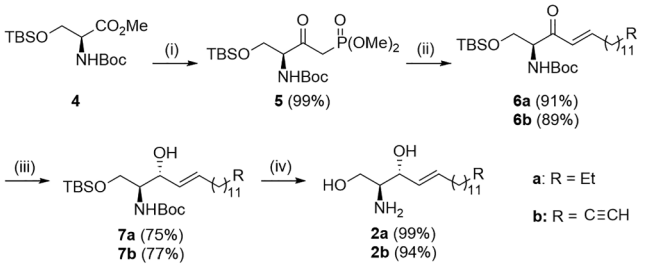

Scheme 1. Synthesis of sphingoid bases **2a** and **2b**. Reagents and conditions: (i) *n*-BuLi, dimethyl methylphosphonate, THF, −78 °C, 2 h; (ii) tetradecanal or tetradec-13-ynal, NEt_3, LiCl, THF, r.t., 24 h; (iii) $LiAlH(OtBu)_3$, EtOH, −78 °C, 1.5 h; (iv) TFA, CH_2Cl_2, r.t., 1 h.

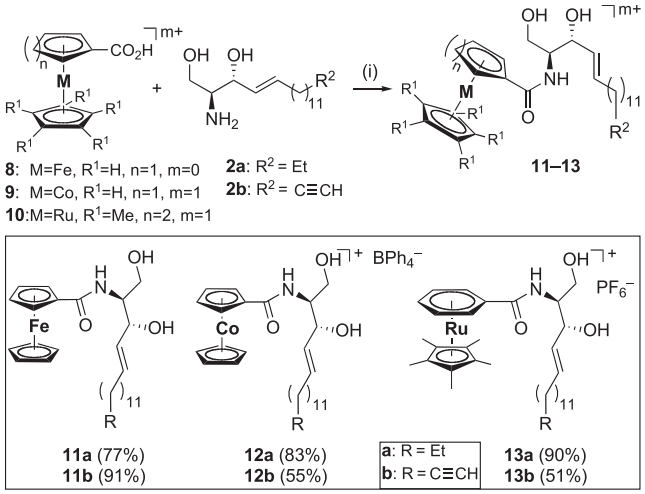

Scheme 2. Synthesis of organometallic ceramide analogues **11**–**13**. Reagents and conditions: (i) HBTU, DIPEA, DMF, 1 h, r.t.

good yields.

To estimate the stability of the *N*-metallocenoylsphingosines **11a**, **12a** and **13a** under biological conditions, UV–vis spectra of their solutions in a water–DMF (99:1) mixture were recorded over the course of 48 h (ESI Figure S1). They showed distinct spectra with a maximum at λ = 240–260 nm (**11a**, **13a**), or two absorption maxima in the same range (**12a**). While the shape of the spectral curves remained largely the same, their height (=absorbance) diminished over time, most rapidly so for the cobalt complex **12a**. This observation can be rationalized by a decreasing concentration of the amphiphilic complexes due to partial precipitation or micelle formation. However, all complexes appear to be sufficiently long-lived to be taken up by cancer cells and to reach their biological targets [32].

2.2. Inhibition of purified acid ceramidase

The *N*-metallocenoylsphingosines **11a**, **12a**, and **13a** were tested for their ability to inhibit human AC (ASAH1) in vitro. Using a fluorescence based assay developed by Bedia et al. [16] we measured the IC_{50} values for the inhibition of AC by complexes **11a**, **12a** and **13a** (Fig. 2). In contrast to the original work by Bedia et al. we expressed human acid ceramidase recombinantly in High Five insect cells and purified the enzyme by affinity chromatography and gel filtration, instead of using a crude cell extract (*cf* Supporting Information). In this way we were able to control the exact amount of enzyme used in our assays, rather than relying on an approximation for its quantification. By a modified variant of Bedia's fluorescence assay, we measured a K_M value of 14 μM for the affinity of our purified enzyme for the Rbm14-12 substrate, compared to 26 μM for the affinity of Bedia's enzyme sample. Using this measured K_M value as a basis for the Rbm14-12 substrate concentration, we found ruthenium complex **13a** (23.5 ± 0.5 μM) to be the best AC inhibitor, while complexes **11a** (142.6 ± 7.6 μM) and **12a**

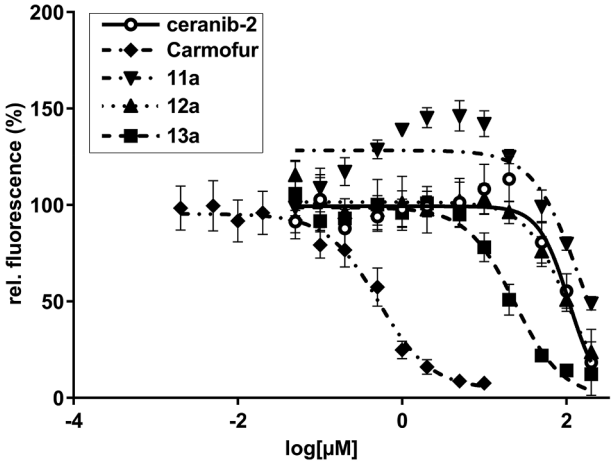

Fig. 2. Inhibition of AC (0.05 μg) after 30 min of incubation with ceranib-2, **11a**, **12a** or **13a** at 37 °C at a final concentration range of 200–0.05 μM, or 10 μM–2 nM of carmofur. Means ± SD from four independent values [16].

(98.1 ± 14.0 μM) were approximately five to seven times less active. The IC_{50} value of *ca.* 110 μM obtained for ceranib-2 under these assay conditions is not reliable due to its limited solubility. In earlier inhibition assays with cellular ceramidase enzymes under less well-defined conditions ceranib-2 was active with an IC_{50} = 28 μM [27]. For the better soluble, known AC-inhibitor carmofur [33] we measured, as expected, a superior activity with IC_{50} = 0.55 ± 0.09 μM.

2.3. Intracellular localization

Acid ceramidases are predominantly found in lysosomes or nuclei of mammalian cells [34–36]. To test if complexes **11a**, **12a** or **13a** not only inhibit AC but actually accumulate in these organelles we treated 518A2 melanoma cells with the alkyne-tagged *N*-metallocenoylsphingosines **11b**, **12b**, and **13b** (30 μM, 0.5 h). Due to the bioorthogonality of the acetylene group, these derivatives behave just like their saturated **a**-analogues. We tracked their intracellular localization by "clicking" them with a mixture of 3-azido-7-hydroxycoumarin, sodium ascorbate and copper sulphate to form a fluorescent triazole which was visualized by confocal fluorescence microscopy (Fig. 3) [37–41]. We found all three complexes to colocalize with lysosomes. The neutral ferrocenoyl complex **11b** was also present in other cell compartments, resulting in a lower Pearson correlation coefficient (PC = 1 for a complete match; PC = 0.56 for **11b**). Due to overlapping fluorescence spectra of the triazole products and stained nuclei, their co-staining was not possible. In contrast to **11b**, the positively charged cobalt and ruthenium complexes **12b** and **13b** were found mainly in the lysosomes, resulting in high values for PC and Li's Intensity Correlation Coefficient (**12b**: PC = 0.92, LICQ = 0.47; **13b**: PC = 0.95, LICQ = 0.42).

2.4. Inhibition of cancer cell growth

Having shown that the *N*-metallocenoylsphingosines inhibit AC and accumulate mainly in AC-rich lysosomes of cancer cells, we studied them for other antitumoral effects and their correlation with AC-inhibition. The cytotoxicities of complexes **11a**, **12a**, **13a** and their alkyne derivatives **11b**, **12b**, **13b**, of sph, and of the known ceramidase inhibitor ceranib-2 were determined in MTT-assays against nine human cancer cell lines of four entities, including the HCT116 p53 knock out mutant HCT116$^{-/-}$ and the P-gp1 overexpressing multi-drug resistant (mdr) cell line KB-V1^{Vbl}. The resulting IC_{50} values are listed in table 1. All complexes were active with IC_{50} values in the low micromolar range. Except for the HCT116 cells, ferrocene **11a** was the most active metal complex. None of the three **a**-type complexes appears to be a substrate of efflux transporter P-gp1 since each showed similar activities against the mdr Kb-V1^{Vbl} cervix carcinoma cells, both in the presence and absence of the competitive P-gp1 inhibitor verapamil. In the HCT116 wildtype cell line (HCT116^{wt}) **12a** was the most active complex, whereas in the p53 knock-out mutant (HCT116$^{-/-}$) Ru complex **13a** was most active, again with low single-digit micromolar IC_{50} values. None of the complexes was as cytotoxic as ceranib-2.

2.5. Cell cycle progression

The effect of **11a**, **12a**, **13a**, sph and ceranib-2 on the cell cycle of 518A2 melanoma cells was investigated by flow cytometry (Fig. 4). Upon treatment for 24 h with varying concentrations, all complexes arrested the melanoma cells in G1-phase. While ferrocene complex **11a** showed effects only at 10 μM, the cobaltocenium and ruthenium arene complexes **12a** and **13a** already had a noticeable impact on the cell cycle at a concentration of 2 μM. This is at variance with the results of the MTT assays. A higher concentration of **11a** was also necessary to cause distinct effects in other biological assays, as discussed below. Compounds **12a** and **13a** seem to arrest the melanoma cells during the G1 phase without causing cell death over the course of 24 h. Sph had a negligible effect on the cell cycle, increasing the cell population in G1-phase only slightly. Ceranib-2 showed the greatest effect, arresting cells at submicromolar concentrations in S- and G2-phase which hints at a different mode of action. Neither sph nor ceranib-2 induced cell death at these concentrations.

2.6. Reactive oxygen species (ROS)

Ceramides can have an indirect impact on the function of membrane associated proteins. Moreover, ceramide accumulation is associated with elevated ROS levels, due to deregulated mitochondrial functions [11]. We monitored ROS levels in 518A2 melanoma cells treated with complexes **11a**, **12a** and **13a** using the nitroblue tetrazolium (NBT) assay. In comparison to the solvent control all complexes caused an increase in ROS levels after 24 h of incubation, accompanied by a reduced cell vitality. Complexes **11a** and **13a** doubled the ROS levels at the highest concentration of 10 μM, which is less than their IC_{50} (24 h) values. In contrast, the cobalt complex **12a** nearly quadrupled the ROS per vital cell at this concentration, which is, however, about twice its IC_{50} (24 h) value (Fig. 5).

2.7. Interference with cytoskeletons

The microtubules and F-actin components of the cytoskeleton of 518A2 melanoma cells, previously treated with complexes **11a**, **12a**, or **13a** at concentrations close to their IC_{50} values, were visualized by immunofluorescence staining and the results were documented in fluorescence images (Fig. 6). While the microtubules were evenly distributed in control cells, they seemed to be focussed near cell nuclei and to radiate toward peripheral cell compartments in cells treated with the metal complexes. The microtubules of cells treated with ruthenium complex **13a** appeared to have lost the regular filamentous structure visible in control cells. All complexes strongly influenced the organization of the actin cytoskeleton, causing stress fiber formation and depolymerization of actin filaments throughout the cells.

As mentioned in the introduction, increased levels of ceramides are frequently associated with Golgi fragmentation. Thus, we examined 518A2 melanoma cells treated with **11a**, **12a** or **13a** for such effects by staining their nuclei with DAPI (blue) and by staining α-*N*-acetylgalactosamine residues in their Golgi apparatus with Alexa Fluor 647 HPA lectin antibody (Supporting Information, Figure S2). In comparison to the control, treated cells indeed revealed a Golgi apparatus that was more diffuse around the nucleus, hinting at its fragmentation.

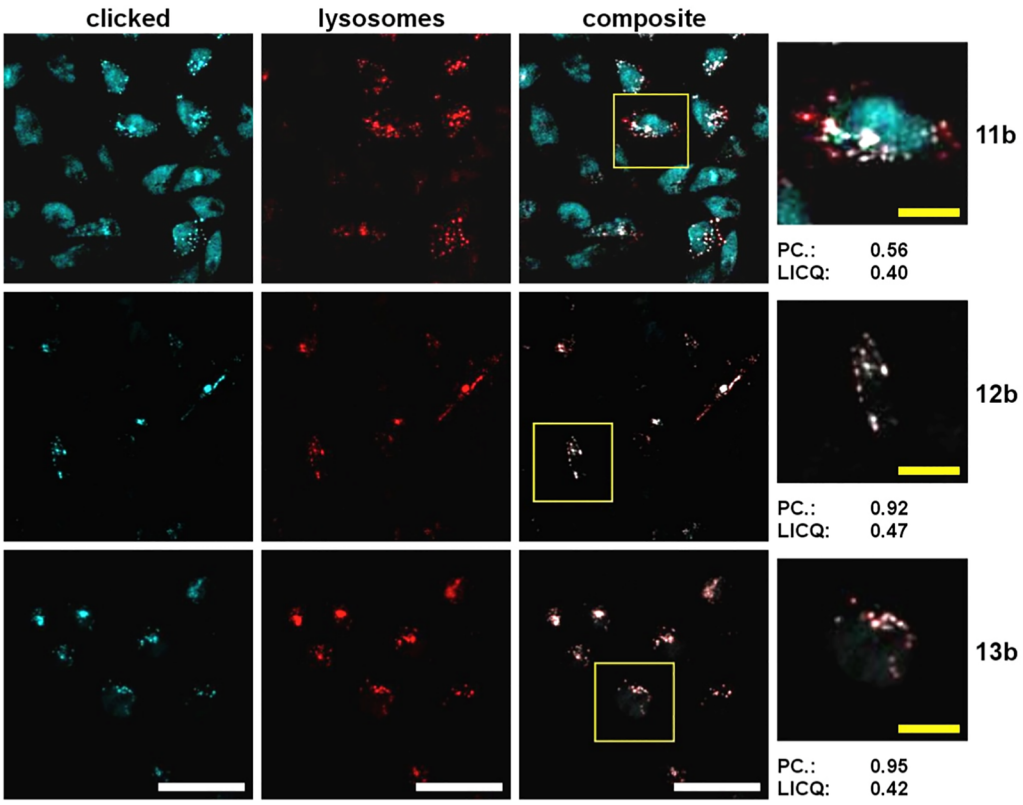

Fig. 3. Colocalization of alkyne-labeled complexes **11b**, **12b**, **13b** (30 μM, 0.5 h) and lysosomes (red) in 518A2 melanoma cells after "click" reaction with 3-azido-7-hydroxycoumarin to give triazoles (cyan). Yellow box: cell that was analyzed for PC and LICQ values using ImageJ (JaCOPI) [42–44]; PC, Pearson Coefficient; LICQ, Li's Intensity Correlation Quotient. Scales: white: 50 μm; yellow 15 μm. (For interpretation of the references to colour in this figure legend, the reader is referred to the web version of this article.)

2.8. Induction of caspase activity

Caspase-3 and -7 are often activated upon deregulation of the cer/s1p rheostat, especially by elevated levels of cer or sph. By means of Apo-One® Homogeneous Caspase-3/-7 Assays (Promega) we ascertained that all complexes **11a**, **12a** and **13a** caused caspase-3/-7 activation in 518A2 melanoma cells, most strongly so the cobaltocenium complex **12a**, which was, however, still inferior to the established apoptosis inducer staurosporine (Fig. 7)

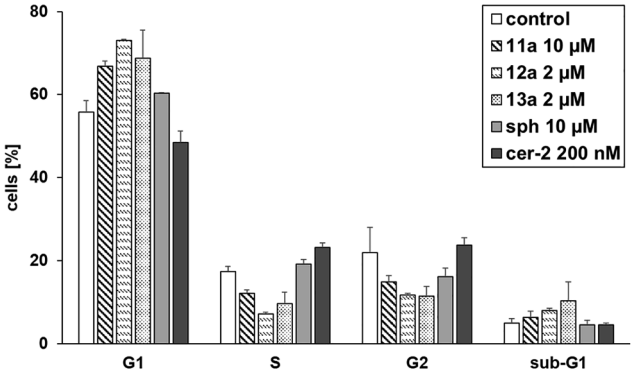

Fig. 4. Cell cycle analysis of 518A2 melanoma cells, treated with **11a** (10 μM), **12a** (2 μM), **13a** (2 μM), sph (10 μM), cer2 = ceranib-2 (200 nM) or the solvent as control for 24 h.

3. Conclusions

The replacement of the fatty acyl residue in ceramides by metallocenoyl residues led to metallodrugs **11–13** with properties distinctly different from those of ceramides. Our main objective, to find new substrate-like, targeted inhibitors of ceramidase was realized with ruthenium complex **13a**. It inhibited purified human AC with an IC_{50} of

Table 1
Means ± SD of IC_{50} values [μM] of compounds **11–13**, sph, and ceranib-2 in MTT assays with human cell lines[a] after 72 h of incubation as calculated from four independent measurements.

	Cell lines									
	518A2	HT-29	HCT116^{wt}	HCT116$^{-/-}$	DLD-1	EaHy.926	U87	Hela	Kb-V1^{Vbl} [b]	Kb-V1$^{Vbl + vpm}$ [b]
11a	5.0 ± 0.1	1.4 ± 0.3	6.6 ± 0.7	11.9 ± 0.2	7.3 ± 0.2	4.7 ± 0.2	3.3 ± 0.7	4.2 ± 0.3	7.5 ± 0.4	4.4 ± 0.5
11b	3.6 ± 0.5	4.1 ± 0.2	10.0 ± 0.1	11.8 ± 0.5	13.0 ± 0.6	6.5 ± 0.3	4.5 ± 0.1	5.7 ± 0.2	7.6 ± 0.9	4.9 ± 0.5
12a	5.8 ± 0.2	4.3 ± 0.5	2.4 ± 0.2	6.3 ± 0.3	10.0 ± 0.4	7.3 ± 0.5	5.7 ± 0.5	10.3 ± 0.8	20.4 ± 0.7	12.0 ± 0.6
12b	5.7 ± 0.8	6.3 ± 0.3	8.9 ± 0.4	3.2 ± 0.7	17.4 ± 1.0	6.6 ± 0.3	8.4 ± 1.0	11.4 ± 1.0	31.2 ± 1.3	24.5 ± 0.4
13a	7.6 ± 0.1	10.6 ± 0.2	9.4 ± 0.3	2.8 ± 0.1	12.8 ± 0.8	5.2 ± 0.6	7.6 ± 1.0	5.6 ± 0.2	27.4 ± 0.4	32.9 ± 1.7
13b	5.7 ± 0.9	27.3 ± 0.5	27.8 ± 0.3	16.9 ± 0.5	20.9 ± 2.2	27.4 ± 0.3	21.5 ± 0.7	28.8 ± 0.4	31.7 ± 3.0	44.2 ± 2.8
sph	11.9 ± 0.9	6.4 ± 0.4	12.7 ± 0.7	15.6 ± 0.7	16.6 ± 1.9	21.8 ± 0.9	19.1 ± 1.5	31.4 ± 0.6	9.5 ± 1.8	4.7 ± 0.4
ceranib-2	0.70 ± 0.03	0.59 ± 0.04	1.2 ± 0.0	0.78 ± 0.05	0.69 ± 0.08	0.20 ± 0.05	3.1 ± 0.2	0.63 ± 0.11	0.79 ± 0.11	0.69 ± 0.02

[a] 518A2 – melanoma, HT-29 – colon adenocarcinoma, HCT116^{wt} – colon carcinoma (wildtype), HCT116$^{-/-}$ - colon carcinoma (p53 knock-out mutant), DLD-1 – Dukes type C colorectal adenocarcinoma, Ea.Hy926 – endothelial hybrid, U87-MG – likely glioblastoma, Hela – cervix carcinoma, Kb-V1^{Vbl} – cervix carcinoma.
[b] Vbl – vinblastine, vpm – verapamil.

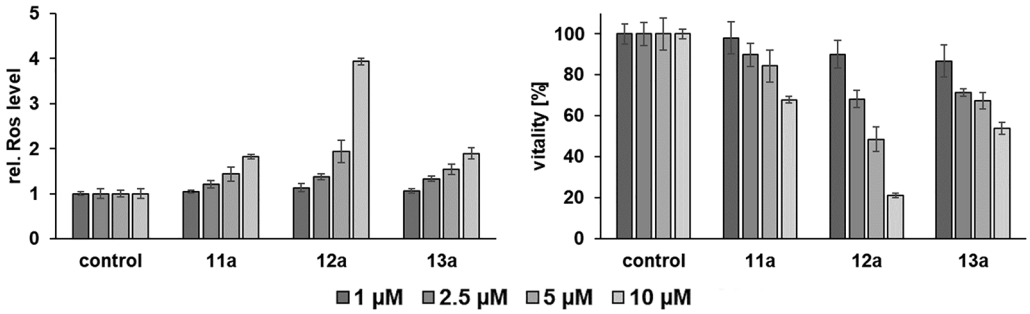

Fig. 5. *Left:* Relative levels of reactive oxygen species (ROS) in 518A2 melanoma cells, after 24 h incubation with 1, 2.5, 5 or 10 µM of **11a**, **12a** or **13a** or the solvent as control, calculated in relation to the percentage of vital cells. *Right:* Vitality of 518A2 melanoma cells from analogously conducted MTT proliferation assays. Means ± SD from three independent values.

ca. 23 µM, a value which, though inferior by a factor of 10 to that of dedicated AC-inhibitors such as carmofur, is pharmacologically meaningful. The distinctly weaker ceramidase inhibition by the neutral ferrocene conjugate **11a** and the "cationic" cobaltocenium derivative **12a** indicates that the steric demand of the arene ligands might be more decisive for their interference with the target enzyme than the complex charge and the nature of the central metal. The complex charge, however, seems to be crucial for the intracellular accumulation: the cationic cobalt and ruthenium complexes readily accumulated in lysosomes, whereas the neutral ferrocene complex **11a** was also found in the cytosol. Thus, our data suggest that the next generation of AC-inhibitors of this type should carry bulky ligands and a positive charge in order to accumulate at sites rich in the target enzyme.

Concerning the antiproliferative activity, the less effective AC-inhibitors **11a** and **12a** were on average slightly more antiproliferative against our cancer cell lines than complex **13a**. This indicates that ceramidase inhibition is only one aspect among several antitumoral factors. All three metallocenoylsphingosines **11–13** showed additional antitumoral effects, whose intensities are also not stringently correlated with their AC-inhibitory potential. For instance, the best AC-inhibitor **13a** also had the most pronounced impact on the cytoskeleton of melanoma cells, while the cobalt complex was the strongest inducer of caspase-3/-7 activity and ROS production in these cells.

The results of this study warrant a broader screening of a library of (cationic) metallocenoylsphingosines with variance in the arene ligands to establish a structure–activity relation and to identify those secondary effects that are most closely associated with AC-inhibition.

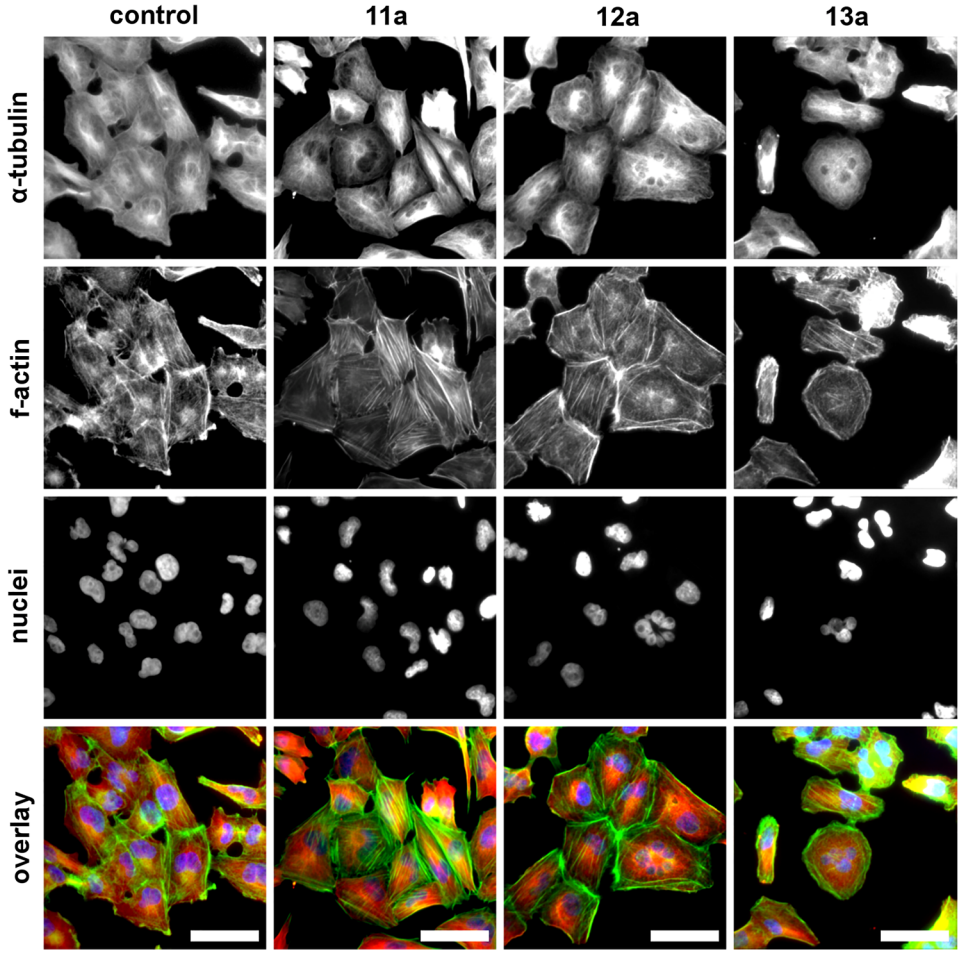

Fig. 6. Immunofluorescence staining of microtubules (red), actin filaments (green) and nuclei (blue) of 518A2 melanoma cells after 24 h of incubation with **11a** (10 µM), **12a** (5 µM), **13a** (5 µM), or the solvent as control. Scale: 50 µm. (For interpretation of the references to colour in this figure legend, the reader is referred to the web version of this article.)

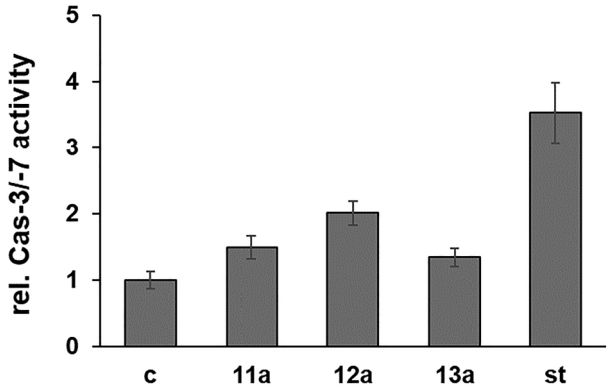

Fig. 7. Activation of caspase-3 and -7 after 4 h of incubation with **11a** (10 μM), **12a** (5 μM), **13a** (5 μM); negative control: DMF; positive control: staurosporine (st, 2 μM). Means ± SD from three independent experiments.

4. Experimental

4.1. Chemistry

Melting points are uncorrected; IR spectra were recorded on an FT-IR spectrometer with ATR sampling unit; NMR spectra were run on a 500 MHz spectrometer; chemical shifts are given in ppm (δ) downfield from tetramethylsilane as internal standard; Mass spectra: direct inlet, EI, 70 eV; HRMS: UPLC/Orbitrap MS system in ESI mode; Microanalyses: Elementar Unicube analyzer. Specific optical rotations were measured at 589 nm (Na-D-line) and are given in deg $cm^3\ g^{-1}\ dm^{-1}$. Absorption and fluorescence measurements were obtained using a plate reader (Tecan Infinite F200). Cell cycle analysis was done using a flow cytometer (Beckman Coulter Cytomics FC500). Fluorescence images were obtained using an AxioCAM MRm (Zeiss, Axioplan2) or a Leica TCS SP5 confocal microscope. Serine ester **4** [45], tetradecanal [46], tetradec-13-ynal [47], **9** [48], **10** [49], and Rbm14-12 [50] were prepared according to literature procedures. All tested compounds were > 95% pure by elemental analysis and/or UPLC–HRMS.

4.1.1. tert-Butyl (S)-(1-((tert-Butyldimethylsilyl)oxy)-4-(dimethoxyphosphoryl) -3-oxobutan-2-yl)carbamate (5)

A solution of dimethyl methylphosphonate (5.34 mL, 49.5 mmol, 3.3 equiv) in THF (150 mL) at −78 °C was treated with *n*-BuLi (2.5 M in hexane, 19.2 mL, 48.0 mmol, 3:2 equiv). After stirring for 30 min, a solution of **4** (5.0 g, 15.0 mmol, 1.0 equiv) in THF (50 mL) was added dropwise. The mixture was stirred for 1 h at −78 °C. Then sat. aq. NH_4Cl (200 mL) was added, the phases were separated, and the aqueous phase was extracted with EtOAc (2 × 100 mL). The combined organic phases were washed with brine (300 mL), dried over $MgSO_4$, and concentrated *in vacuo*. The crude product was purified by flash chromatography (silica gel, *n*-hexane/ethyl acetate 1:1) to give **5** as a colorless oil. Yield: 6.31 g (14.8 mmol, 99%). $[\alpha]_D^{23}$ = +62.3 (c = 1.0, $CHCl_3$). ^{1}H NMR (500 MHz, $CDCl_3$): δ = 5.53 (d, J = 7.6 Hz, 1H), 4.41–4.49 (m, 1H), 4.07 (dd, J = 10.4, 3.7 Hz, 1H), 3.84 (dd, J = 10.4, 4.0 Hz, 1H), 3.80 (d, J = 2.9 Hz, 3H), 3.78 (d, J = 2.9 Hz, 3H), 3.41 (dd, J = 22.0, 14.6 Hz, 1H), 3.14 (dd, J = 22.0, 14.6 Hz, 1H), 1.45 (s, 9H), 0.86 (s, 9H), 0.04 (s, 6H). ^{13}C NMR (126 MHz, $CDCl_3$): δ = 199.7, 155.2, 79.9, 63.0, 61.9, 60.4, 53.1, 38.5 (d, ^1J(C,P) = 131.7 Hz), 28.3, 25.7, 18.2, −5.6. HRMS (ESI): *m/z* calculated for $C_{17}H_{36}O_7NPSi + Na^+$ [M + Na^+]: 448.1891. Found: 448.1890.

4.1.2. tert-Butyl (S,E)-(1-((tert-Butyldimethylsilyl)oxy)-3-oxooctadec-4-en-17-yn-2-yl)carbamate (6b)

NEt_3 (3.1 mL, 22.44 mmol, 3.0 equiv) was added to a solution of **5** (3.18 g, 7.46 mmol, 1.0 equiv), LiCl (0.95 g, 22.44 mmol, 3.0 equiv) and tetradec-13-ynal (3.12 g, 15.0 mmol, 2.0 equiv) in THF (150 mL) and the resulting mixture was stirred at room temperature for 18 h. Then 1 M citric acid (150 mL) was added, the phases were separated and the aqueous phase was extracted with EtOAc (2 × 100 mL). The combined organic phases were washed with brine (300 mL), dried over $MgSO_4$, and concentrated *in vacuo*. The crude product was purified by flash chromatography (silica gel, *n*-hexane/ethyl acetate 30:1) to leave **6b** as a colorless oil. Yield: 3.38 g (6.66 mmol, 89%). $[\alpha]_D^{23}$ = +43.4 (c = 1.1, $CHCl_3$). ^{1}H NMR (500 MHz, $CDCl_3$): δ = 6.95 (dt, J = 15.8, 7.0 Hz, 1H), 6.26 (d, J = 15.8 Hz, 1H), 4.53 (dt, J = 7.4, 4.0 Hz, 1H), 3.96 (dd, J = 10.4, 4.0 Hz, 1H), 3.82 (dd, J = 10.4, 4.0 Hz, 1H), 2.21 (q, J = 7.0 Hz, 2H), 2.17 (td, J = 7.1, 2.6 Hz, 2H), 1.92 (t, J = 2.6 Hz, 1H), 1.47–1.55 (m, 2H), 1.43 (m, 11*H*), 1.34–1.40 (m, 2H), 1.22–1.32 (m, 12H), 0.81–0.85 (m, 9H), −0.01 (m, 6H). ^{13}C NMR (126 MHz, $CDCl_3$): δ = 196.4, 155.3, 149.2, 126.9, 79.6, 68.0, 63.6, 59.4, 32.6, 29.5, 29.4, 29.35, 29.2, 29.1, 28.7, 28.35, 28.3, 28.0, 25.7, 18.4, 18.2. HRMS (ESI): *m/z* calculated for $C_{29}H_{53}O_4NSi + Na^+$ [M + Na^+]: 530.3636. Found: 530.3627.

4.1.3. tert-Butyl ((2S,E)-1-((tert-Butyldimethylsilyl)oxy)-3-hydroxyoctadec-4-en-17-yn-2-yl)carbamate (7b)

7b was prepared according to a literature procedure [31] from **6b** (1.33 g, 2.60 mmol, 1.0 equiv) and $LiAlH(O^tBu)_3$ (1.32 g, 5.20 mmol, 2.0 equiv) as a colorless oil. Yield: 1.02 g (2.00 mmol, 77%). $[\alpha]_D^{23}$ = +16.6 (c = 1.0, $CHCl_3$). ^{1}H NMR (500 MHz, $CDCl_3$): δ = 5.75 (dtd, J = 15.3, 6.9, 0.9 Hz, 1H), 5.50 (dd, J = 15.3 Hz, 5.9, 2H), 5.24 (d, J = 8.2 Hz, 1H), 4.16–4.22 (m, 1H), 3.93 (dd, J = 10.2, 3.1 Hz, 1H), 3.75 (dd, J = 10.2, 2.4 Hz, 1H), 3.53–3.60 (m, 1H), 3.33 (d, J = 8.24 Hz, 1H), 2.17 (dt, J = 7.2, 2.7 Hz, 2H), 2.03 – 2.07 (m, 2H), 1.93 (t, J = 2.7 Hz, 1H), 1.48–1.55 (m, 2H), 1.44 (s, 9H), 1.33–1.41 (m, 4H), 1.26 (br. s., 12H), 0.89 (s, 9H), 0.06 (d, J = 1.53 Hz, 6H). ^{13}C NMR (126 MHz, $CDCl_3$): δ = 155.8, 133.0, 129.4, 84.8, 79.4, 74.66, 68.0, 63.5, 54.4, 32.3, 29.6, 29.55, 29.5, 29.2, 29.1, 28.7, 28.5, 28.4, 25.8, 18.4, 18.1. HRMS (ESI): *m/z* calculated for $C_{29}H_{55}O_4NSi + Na^+$ [M + Na^+]: 532.3793. Found: 532.3784.

4.1.4. (2S,E)-2-Aminooctadec-4-en-17-yne-1,3-diol (2b)

TFA (20 mL) was added to a solution of **7b** (1.89 g, 3.73 mmol, 1.0 equiv) in CH_2Cl_2 (20 mL) at 0 °C. The mixture was stirred at room temperature for 1.5 h. Volatiles were removed *in vacuo*. To remove excess TFA the residue was dissolved in MeOH (10 mL) and concentrated at reduced pressure. This was repeated twice. The remaining residue was dissolved in 1 M NaOH (10 mL) and extracted with EtOAc (3 × 10 mL). The combined organic phases were dried over $MgSO_4$ and concentrated *in vacuo*. The crude product was purified by flash chromatography (silica gel, $CHCl_3$/MeOH/NH_4OH 95:5:1) to give 2b as a white solid. Yield: 1.04 g (3.50 mmol, 94%). mp = 69 °C. $[\alpha]_D^{23}$ = +8.9 (c = 1.0, $CHCl_3$). ^{1}H NMR (500 MHz, $CDCl_3$): δ = 5.76 (dtd, J = 15.5, 6.8, 0.6 Hz, 1H), 5.47 (ddt, J = 15.5, 6.8, 1.2 Hz, 1H), 4.05 (t, J = 6.8 Hz, 1H), 3.66 (qd, J = 10.8, 5.3 Hz, 2H), 2.86 (q, J = 5.3 Hz, 1H), 2.18 (td, J = 7.2, 2.7 Hz, 2H), 2.06 (q, J = 6.8 Hz, 2H), 1.94 (t, J = 2.7 Hz, 1H), 1.48–1.58 (m, 2H), 1.34–1.43 (m, 4H), 1.24–1.33 ppm (m, 12H). ^{13}C NMR (126 MHz, $CDCl_3$) δ = 134.7, 129.3, 84.8, 75.5, 68.0, 64.1, 56.1, 32.3, 29.55, 29.5, 29.4, 29.2, 29.1, 28.7, 28.6, 18.4. HRMS (ESI): *m/z* calculated for $C_{18}H_{34}O_2N$ [M + H^+]: 296.2576. Found: 296.2584.

4.1.5. General procedure for the synthesis of complexes 11–13 from 2

To a solution of the respective organometallic carboxylic acid **8–10** (1.0 equiv) in dry dimethylformamide (0.05 M), diisopropylethylamine (2.0 equiv), HBTU (1.1 equiv) and the corresponding sphingoid base **2** (1.1 equiv) were added at 0 °C. The mixture was stirred for 1 h while it was allowed to reach room temperature. Volatiles were removed under reduced pressure and the remainder was dissolved in CH_2Cl_2 (10 mL), washed with 1 M NaOH (10 mL), 1 M aqueous HCl (10 mL), and water (10 mL). The organic phase was dried ($MgSO_4$) and evaporated to dryness.

4.1.6. N-((2S,3R,E)-1,3-Dihydroxyoctadec-4-en-2-yl) ferrocenecarboxamide (11a)

11a was prepared according to the general procedure from **8** (50 mg, 0.22 mmol), DIPEA (74 μL, 0.43 mmol), HBTU (91 mg, 0.24 mmol) and **2a** (71 mg, 0.24 mmol). The crude product was purified by flash chromatography (silica gel, *n*-hexane/acetone 2:1) to give an orange solid. Yield: 86 mg (0.17 mmol, 77%). mp = 81 °C. $[\alpha]_D^{23}$ = +7.7 (c = 0.2, $CHCl_3$). ^{1}H NMR (500 MHz, $CDCl_3$): δ = 6.58 (d, J = 7.6 Hz, 1H), 5.83 (dt, J = 15.5, 7.0 Hz, 1H), 5.57 (dd, J = 15.5, 6.4 Hz, 1H), 4.71 (d, J = 8.9 Hz, 2H), 4.39 – 4.37 (m, 1H), 4.35 (s, 2H), 4.20–4.23 (m, 5H), 4.01–4.06 (m, 1H), 3.96 (dd, J = 11.3, 4.0 Hz, 1H), 3.76 (dd, J = 11.3, 2.7 Hz, 1H), 3.56 (br. s., 2H), 2.06 (q, J = 7.0 Hz, 2H), 1.33–1.41 (m, 2H), 1.20–1.32 (m, 20H), 0.87 ppm (t, J = 6.9 Hz, 3H). ^{13}C NMR (126 MHz, $CDCl_3$): δ = 171.6, 134.2, 128.8, 75.3, 74.1, 70.7, 69.9, 68.4, 68.3, 62.4, 54.9, 32.3, 31.9, 29.7, 29.6, 29.6, 29.5, 29.3, 29.2, 29.2, 22.7, 14.1. MS (ESI +): m/z 512,4 [M+H$^+$]. Elemental analysis calculated (%) for $C_{29}H_{45}FeNO_3$: C 68.09, H 8.87, N 2.74. Found: C 68.33, H 8.60, N 3.01.

4.1.7. N-((2S,3R,E)-1,3-Dihydroxyoctadec-4-en-17-yn-2-yl) ferrocenecarboxamide (11b)

11b was prepared according to the general procedure from **8** (50 mg, 0.22 mmol), DIPEA (74 μL, 0.43 mmol), HBTU (91 mg, 0.24 mmol) and **2b** (71 mg, 0.24 mmol). The crude product was purified by flash chromatography (silica gel, *n*-hexane/acetone 2:1) to leave an orange solid. Yield: 100 mg (0.20 mmol; 91%). mp = 67 °C. $[\alpha]_D^{23}$ = +12.5 (c = 0.2, $CHCl_3$). ^{1}H NMR (500 MHz, $CDCl_3$): δ = 6.51 (d, J = 7.0 Hz, 1H), 5.86 (dt, J = 15.6, 7.0 Hz, 1H), 5.61 (dd, J = 15.6, 6.4 Hz, 1H), 4.70–4.73 (m, 2H), 4.42–4.47 (m, 1H), 4.36–4.39 (m, 2H), 4.24 (s, 5H), 4.01–4.08 (m, 2H), 3.78–3.84 (m, 1H), 2.78–2.83 (m, 2H), 2.19 (td, J = 7.1, 2.6 Hz, 2H), 2.10 (q, J = 7.0 Hz, 2H), 1.95 (t, J = 2.6 Hz, 1H), 1.49–1.57 (m, 2H), 1.36–1.44 (m, 4H), 1.24–1.33 ppm (m, 12H). ^{13}C NMR (126 MHz, $CDCl_3$): δ = 171.3, 134.4, 128.9, 74.7, 70.6, 69.8, 68.3, 68.2, 68.0, 62.6, 54.7, 32.3, 29.6, 29.5, 29.4, 29.2, 29.1, 28.7, 28.5, 18.4. MS (ESI$^+$): m/z 508.4 [M+H$^+$]. Elemental analysis calculated (%) for $C_{29}H_{41}FeNO_3$: C 68.63, H 8.14, N 2.76. Found: C 68.89, H 8.46, N 2.88.

4.1.8. N-((2S,3R,E)-1,3-Dihydroxyoctadec-4-en-2-yl)cobaltoceniumcarboxamide Tetraphenylborate (12a)

12a was prepared according to the general procedure from **9** (100 mg, 0.26 mmol), DIPEA (90 μL, 0.53 mmol), HBTU (109 mg, 0.29 mmol) and **2a** (110 mg, 0.29 mmol). The crude product was dissolved in 3 mL MeOH followed by the addition of 90 mg of $NaBPh_4$ (0.26 mmol, 1.0 equiv) in 2 mL MeOH. A yellow precipitate formed, which was isolated by filtration, washed with MeOH (5 mL) and dried *in vacuo* to give a yellow solid. Yield: 184 mg (83%). mp = 109 °C. $[\alpha]_D^{23}$ = +25.2 (c = 0.2, $CHCl_3$). ^{1}H NMR (500 MHz, acetone-d_6): δ = 7.74 (d, J = 8.9 Hz, 1H), 7.35 (m, 8H), 6.94 (t, J = 7.5 Hz, 8H), 6.76–6.82 (m, 4H), 6.35–6.37 (m, 1H), 6.32 (m, 1H), 5.83 (s, 5H), 5.80 (t, J = 2.1 Hz, 2H), 5.74 (dt, J = 15.6, 7.0 Hz, 1H), 5.60 (dd, J = 15.6, 6.1 Hz, 1H), 4.24–4.30 (m, 1H), 4.11–4.18 (m, 1H), 3.98 (t, J = 5.5 Hz, 1H), 3.77–3.88 (m, 2H), 2.08–2.03 (m, 2H), 1.33–1.40 (m, 2H), 1.22–1.32 (m, 20H), 0.88 ppm (t, J = 7.0 Hz, 3H). ^{13}C NMR (126 MHz, acetone-d_6): δ = 165.9, 165.5, 165.1, 164.7, 162.6, 137.4, 137.4, 133.9, 131.8, 126.4, 122.7, 95.5, 87.6, 87.4, 87.3, 85.6, 85.2, 73.5, 61.8, 57.9, 33.4, 33.0, 30.8, 30.7, 30.6, 30.4, 30.3, 30.1, 30.0, 29.8, 23.7, 14.8. MS (ESI$^+$): m/z 514,3 [M - BPh_4^-]. MS (ESI$^-$): m/z 319.1 [BPh_4^-]. Elemental analysis calculated (%) for $C_{53}H_{65}BCoNO_3$: C 76.34, H 7.86, N 1.68. Found: C 76.44, H 7.54, N 2.08.

4.1.9. N-((2S,3R,E)-1,3-Dihydroxyoctadec-4-en-17-yn-2-yl) Cobaltoceniumcarboxamide tetraphenylborate (12b)

12b was prepared according to the general procedure from **9** (50 mg, 0.13 mmol), DIPEA (45 μL, 0.26 mmol), HBTU (55 mg, 0.14 mmol) and **2b** (42 mg, 0.14 mmol). The crude product was dissolved in 3 mL MeOH followed by the addition of 45 mg of $NaBPh_4$ (0.13 mmol, 1.0 equiv) in 2 mL MeOH. A yellow precipitate formed, which was isolated by filtration, washed with MeOH (5 mL) and dried *in vacuo* to leave a yellow solid. Yield: 59 mg (55%). mp = 97.5 °C. $[\alpha]_D^{23}$ = +27.5 (c = 0.2, $CHCl_3$). ^{1}H NMR (500 MHz, acetone-d_6): δ = 7.70–7.80 (m, 1H), 7.32–7.39 (m, 8H), 6.94 (t, J = 7.5 Hz, 8H), 6.77–6.82 (m, 6H), 6.34–6.38 (m, 1H), 6.30–6.33 (m, 1H), 5.81–5.84 (m, 5H), 5.80 (t, J = 2.1 Hz, 2H), 5.71–5.78 (m, 1H), 5.60 (dd, J = 15.3, 6.1 Hz, 1H), 4.24–4.29 (m, 1H), 4.11–4.19 (m, 1H), 3.97 (t, J = 5.3 Hz, 1H), 3.76–3.89 (m, 2H), 2.31 (t, J = 2.7 Hz, 1H), 2.16 (td, J = 7.0, 2.7 Hz, 2H), 2.01–2.09 (m, 2H), 1.45–1.53 (m, 2H), 1.22–1.44 ppm (m, 16H). ^{13}C NMR (126 MHz, acetone-d_6): δ = 165.9, 165.5, 165.2, 164.8, 162.6, 137.5, 133.9, 131.9, 126.5, 122.8, 87.6, 87.4, 87.3, 85.6, 85.2, 73.5, 70.3, 61.9, 57.9, 33.4, 30.8, 30.7, 30.6, 30.5, 30.3, 30.1, 30.0, 29.9, 29.8, 19.1. MS (ESI$^+$): m/z 510.3 [M − BPh_4^-]. MS (ESI$^-$): m/z 319.1 [BPh_4^-]. Elemental analysis calculated (%) for $C_{53}H_{61}BCoNO_3$: C 76.71, H 7.41, N 1.67. Found: C 76.77, H 7.85, N 2.03.

4.1.10. {η6-[N-((2S,3R,E)-1,3-dihydroxyoctadec-4-en-17-yn-2-yl) benzamide)]}(η5-1,2,3,4,5-pentamethylcyclopentadienyl)-ruthenium (13a)

13a was prepared according to the general procedure from **10** (50 mg, 0.10 mmol), DIPEA (34 μL, 0.20 mmol), HBTU (42 mg, 0.11 mmol) and **2a** (33 mg, 0.11 mmol). The crude product was purified by flash chromatography (silica gel, CH_2Cl_2/MeOH 95:5) to give a white solid. Yield: 70 mg (0.05 mmol, 90%). mp = 129 °C. $[\alpha]_D^{23}$ = +7.5 (c = 0.2, $CHCl_3$). ^{1}H NMR (500 MHz, $CDCl_3$): δ = 7.42 (d, J = 7.9 Hz, 1H), 6.36–6.45 (m, 2H), 5.79–5.97 (m, 4H), 5.54 (dd, J = 15.6, 6.1 Hz, 1H), 4.39–4.44 (m, 1H), 4.00–4.09 (m, 2H), 3.81 (d, J = 8.2 Hz, 1H), 2.00–2.08 (m, 2H), 1.87–1.96 (m, 15H), 1.32–1.39 (m, 2H), 1.18–1.31 (m, 26H), 0.87 (t, J = 7.3 Hz, 3H). ^{13}C NMR (126 MHz, $CDCl_3$): δ = 163.3, 134.0, 128.5, 97.8, 92.3, 88.3, 87.2, 87.1, 85.6, 85.4, 74.0, 61.7, 55.9, 32.3, 31.9, 29.7, 29.6, 29.6, 29.5, 29.5, 29.3, 29.3, 29.2, 29.1, 22.7, 14.1, 10.1. MS (ESI$^+$): m/z 640.4 [M − PF_6^+]. MS (ESI$^-$): m/z 144.9 [PF_6^-]. Elemental analysis calculated (%) for $C_{35}H_{56}F_6NO_3PRu$: C 53.56, H 7.19, N 1.78. Found: C 53.28, H 7.28, N 2.07.

4.1.11. {η6-[N-((2S,3R,E)-1,3-Dihydroxyoctadec-4-en-17-yn-2-yl) benzamide)]}(η5-1,2,3,4,5-pentamethylcyclopentadienyl)ruthenium (13b)

13b was prepared according to the general procedure from **10** (50 mg, 0.10 mmol), DIPEA (34 μL, 0.20 mmol), HBTU (42 mg, 0.11 mmol) and **2b** (32 mg, 0.11 mmol). The crude product was purified by flash chromatography (silica gel, CH_2Cl_2/MeOH 98:2) to leave a white solid. Yield: 40 mg (0.05 mmol, 51%). mp = 118 °C. $[\alpha]_D^{23}$ = +6.5 (c = 0.2, $CHCl_3$). ^{1}H NMR (500 MHz, $CDCl_3$): δ = 7.35 (d, J = 7.6 Hz, 1H), 6.41 (dd, J = 14.5, 6.0 Hz, 2H), 5.91–5.96 (m, 1H), 5.80–5.91 (m, 3H), 5.55 (dd, J = 15.4, 6.0 Hz, 1H), 4.44 (s, 1H), 4.01–4.10 (m, 2H), 3.80–3.88 (m, 1H), 3.40 (br. s, 1H), 3.12–3.24 (br. m, 1H), 2.18 (td, J = 7.1, 2.6 Hz, 2H), 2.02–2.10 (m, 2H), 1.95 (s, 16H), 1.53 (quin, J = 7.3 Hz, 2H), 1.33–1.43 (m, 4H), 1.22–1.32 ppm (m, 12H). ^{13}C NMR (126 MHz, $CDCl_3$): δ = 163.2, 134.1, 128.4, 97.8, 92.3, 88.2, 87.1, 85.6, 85.4, 84.8, 74.0, 68.0, 61.7, 55.8, 32.3, 29.6, 29.5, 29.2, 29.1, 28.7, 28.5, 18.4, 10.1. MS (ESI$^+$): m/z 636.4 [M − PF_6^-]. MS (ESI$^-$): m/z 144.9 [PF_6^-]. Elemental analysis calculated (%) for $C_{35}H_{52}F_6NO_3PRu$: C 53.84, H 6.71, N 1.79. Found: C 53.55, H 6.85, N 2.13.

4.2. Biological evaluation

4.2.1. Recombinant expression of ASAH1 in High Five insect cells

Recombinant full length ASAH1 was expressed and secreted from High Five insect cells. The used vector containing the genetic information for ASAH1 was obtained from Genescript. The first 21 amino acids were exchanged for the melittin signal sequence (MKFLVNVALVFMVVYISYIYA) [51]. At the C-terminus a TEV site, followed by a His-

tag (ENLYFQGGGGHHHHHH) was added. 48 h after infection with the respective baculovirus, the cells (1.2 mio cells/mL) were centrifuged (4500 rpm, 4 °C, 5 min), and the supernatant containing the secreted ASAH1 was dialysed against Ni^{2+}-IMAC binding buffer (50 mM NaH_2PO_4, 300 mM NaCl, pH 7.8, 4 × 1 L, 4 °C). After dialysis, Ni^{2+}-IMAC was performed (washing buffer 50 mM NaH_2PO_4, 300 mM NaCl, 20 mM imidazol, pH 7.8; elution buffer 50 mM NaH_2PO_4, 300 mM NaCl, 125 mM imidazole, pH 7.8). The protein was concentrated (amicon stirred cell, NADIR/UP020P) and the protein was further purified via gel filtration (flow 0.6 mL/min, Hiload 16/600 Superdex 200 pg, buffer 50 mM Tris/HCl, 200 mM NaCl, pH 7.6). The purity of the protein was determined via SDS-page (*cf.* Supporting Information) The protein concentration was determined at A280 using the extinction coefficient $\varepsilon = 79215\ M^{-1}\ cm^{-1}$. From 320 mL of medium we obtained 2.4 mg of pure enzyme.

4.2.2. Determination of K_M of the fluorescence substrate Rbm14-12

The assay for the determination of the K_M and IC_{50} values is based on the fluorescence assay of Bedia et al. [16]. In 1.5 mL Eppendorf reaction tubes 750 µL of reaction mix containing 645 µL NaOAc buffer (25 mM, pH 4.5), 5 µL of Rbm14-12 predilutions in EtOH (final concentrations 0, 2.5, 5, 7.5, 10, 20, 40, 60 µM, 0.5% EtOH) were prepared. The reactions were started with 250 µL of ASAH1 solution in NaOAc buffer (final concentration 500 ng/mL). The reaction tubes were incubated at 37 °C. After 0, 5, 10, 15, 20, 30, 40, and 50 min, 100 µL samples were withdrawn from each tube and added to 50 µL of MeOH in the wells of a 96 black well plate to stop the enzyme reaction. 100 µL of a 2.5 mg/mL $NaIO_4$ solution (100 mM glycine/NaOH, pH 10.6) were added to each well and the plate was incubated at room temperature in the dark for 2 h. For background measurements reaction tubes containing blanks were treated analogously. The fluorescence of the resulting umbelliferone was measured at $\lambda_{ex} = 340$ and $\lambda_{em} = 465$ nm. The K_M value (*cf.* Supporting Information) was determined using *GraphPad Prism*.

4.2.3. Determination of ceramidase inhibition (IC50 values)

In a 96 black well plate 75 µL of reaction mix, containing 64.5 µL NaOAc buffer (25 mM, pH 4.5), 0.5 µL of fluorescence substrate Rbm14-12 (final concentration 14 µM), and 10 µL of a predilution of **11a**, **12a**, **13a**, carmofur, ceranib-2 or the solvent in NaOAc buffer (final concentrations 200 µM to 50 nM, or 10 µM to 2 nM in the case of carmofur) were prepared. The enzyme reaction was started by addition of 25 µL of NaOAc containing 0.05 µg ASAH1, resp. 25 µL of pure NaOAc for background fluorescence determination, into each well. The reaction was stopped after 30 min (37 °C) by addition of 50 µL of MeOH to each well. Then 100 µL of a 2.5 mg/mL $NaIO_4$ solution (100 mM glycine/NaOH, pH 10.6) were added into each well and the plate was incubated at room temperature in the dark for 2 h. The fluorescence of the product umbelliferone was measured at 340 nm_{ex} / 465 nm_{em}. IC_{50} values (means ± SD) were calculated from four independent values using *GraphPad Prism*. We checked that the metal complexes do not themselves interfere with the fluorescence intensity of umbelliferone (*cf.* Figure S5).

4.2.4. Cell culture conditions

The cell lines used for the biological evaluation were cultivated in *Dulbecco's Modified Eagle Medium* (DMEM) containing 10% FBS and 1% Antibiotic-Antimycotic. The cells were cultivated at 37 °C, 5% CO_2 and 95% humidity.

4.2.5. Intracellular colocalization

518A2 cells were seeded at a density of 0.03×10^6 cells per mL (cpm) onto glass cover slips (Ø 12 mm) inside the wells of a 24 well plate (0.5 mL/well). After 24 h of incubation under cell culture conditions the medium was exchanged for 500 µL of complete DMEM containing 6 µL of Cell light Lysosomes-RFP, BacMam (Thermo Fisher) and the plate was again incubated for 24 h. The cells were treated with 30 µM of **11b**, **12b** or **13b** for 30 min at 37 °C. The old medium was discarded and the cells were washed three times with 1 mL of PBS. After fixation (4% formaldehyde in PBS) for 20 min and permeabilization (0.5% Triton X-100, 1% BSA in PBS), 200 µL of click working solution (2 mM $CuSO_4$, 5 mM sodium ascorbate, 0.1 mM 3-azido-7-hydroxycoumarin, 1% BSA in PBS) were added into each well. The cells were incubated at room temperature in the dark for 30 min before the solution was discarded once more. The cells were washed twice with PBS (1% BSA) before the coverslips were embedded in mowiol. Fluorescence images were taken using a Leica TCS SP5 confocal microscope (pinhole at 1 Airy). Colocalization parameters were calculated for one cell using the ImageJ plugin JaCOP [42–44].

4.2.6. IC_{50} determination using the MTT assay

The cytotoxicity of **11–13**, sph and ceranib-2 was evaluated via MTT based proliferation assays. Cells were seeded at 0.05×10^6 cpm or 0.1×10^6 cpm (DLD-1) into the wells of 96 well plates (100 µL/well) and incubated for 24 h to establish confluency. Appropriate predilutions in H_2O made from fresh stock solutions (10 mM) in DMF or DMSO (ceranib-2) or EtOH (sph) were added into the wells to reach final concentrations ranging from 25 nM to 100 µM. After 72 h of incubation at 37 °C the plates were centrifuged for 5 min (300 g, 4 °C) and the medium was discarded by swiftly turning the plates onto fresh cell tissue paper. 50 µL of an MTT solution (0.05% in PBS) was added into each well and the plates were further incubated at 37 °C for 2 h. The MTT solution was removed as before, and the cells and the formazan were lysed by addition of 25 µL of SDS/DMSO (1%, 0.6% acetic acid). For complete solution of the formazan the plates were incubated for at least another hour at 37 °C before the absorptions of the formazan and the background were measured at 570 nm, respectively at 630 nm. The vitality of the cells treated with the solvent was set to 100% viable cells for each concentration and the vitality of the cells inside the wells treated with **11**, **12, 13** was calculated accordingly. The IC_{50} values were finally calculated via *GraphPad Prism*. Means ± SDs were calculated from four independent values.

4.2.7. Cell cycle analysis

The effects of **11–13**, sph, and ceranib-2 on the progression of the cell cycle of 518A2 melanoma cells were analyzed via propidium iodide (PI) staining and flow cytometry. Cells were seeded at 0.05×10^6 cpm into the wells of 6-well plates (3 mL/well) and the plates were incubated under standard cell culture conditions for 24 h. Dilutions of the test complexes in H_2O were added to the wells to reach final concentrations of 10 µM (**11a**, sph), 2 µM (**12a**, **13a**), 200 nM (ceranib-2) or equal amounts of the respective solvent. The cells were incubated for another 24 h before the medium of each well (3 wells per concentration) was transferred into an ice cooled centrifugation tube, the cells were washed with 1 mL of PBS which was transferred into the respective tube as well. The cells were harvested via trypsination and thorough washing of the wells with PBS, and were transferred into the respective tube. The cells were centrifuged at 300 g (5 min, 4 °C) and the supernatant was discarded. The resulting pellet was resuspended in 1 mL of ice cold EtOH (70%) and kept on ice for at least 1 h. For PI staining the cells were centrifuged at 400 g (5 min, 23 °C) and the supernatant was discarded. The cells were layered with 1 mL PBS and incubated for 5 min at 23 °C. After centrifugation (5 min, 400 g, 4 °C) the PBS was discarded and the pellet was resuspended with 200 µL of PI staining buffer (50 µg/mL propidium iodide, 0.1% sodium citrate, 50 µg/mL RNAse I) and the cells were incubated for 30 min at 37 °C. Thereafter, flow cytometry measurements were done with a Cytomics™ FC 500.

4.2.8. (Immuno-)fluorescence staining

518A2 cells were seeded at 0.05×10^6 cpm analogously to the preparation of the colocalization. The cells were incubated at standard

cell culture conditions for 24 h and then treated with **11a** (10 μM), **12a** (5 μM), **13a** (5 μM) for another 24 h. The medium was removed and the cells were washed thrice with PBS. After fixation with 3.7% formaldehyde in PBS for 20 min at room temperature, the cells were again washed three times with PBS.

Microtubules. For staining of the microtubules the cells were incubated for 30 min (room temperature) with blocking and permeabilization buffer (1% BSA , 0.1% Triton X-100 in PBS). The buffer was replaced with the primary mouse anti-tubulin antibody (1:500 in 1% BSA in PBS) and the plates were incubated for 1 h at 37 °C. The buffer was discarded and the cells were washed three times with PBS, before the secondary goat anti-mouse phalloidin 488 antibody (1:500 in 1% BSA in PBS) was added to each well. After another hour of incubation at room temperature and in the dark, the buffer was discarded again and the cells were washed twice with PBS before the coverslips were layered with 500 μL of sterile water. The coverslips were carefully embedded into mowiol mounting buffer (2.5% DABCO, 1 mg/mL DAPI) and stored at 4 °C.

Actin filaments. Staining of the actin filaments was done using Actin-stain™ 488 phalloidin (Cytoskeleton) and following the protocol provided by the manufacturer. After staining the cells were washed and the coverslips embedded as described above.

Golgi apparatus. Staining of the Golgi apparatus was done similar to microtubule staining. After treatment with the complexes, the cells were fixed and permeabilized as before. The Golgi apparatus was stained using Lectin HPA Alexa Fluor 647 conjugate (20 μg/mL in PBS) for 30 min (room temperature). The cells were embedded as before.

4.2.9. ROS level determination

The generation of reactive oxygen species was monitored by means of Nitro blue tetrazolium chloride (NBT) assays in 518A2 melanoma cells after 24 h of incubation with **11a**, **12a**, **13a**. NBT is reduced to a formazan by reactive oxygen species. The cells were seeded at 0.1×10^6 cells/mL intro the wells of a 96-well plate (100 μL/well) and incubated for 24 h at 37 °C. Appropriate dilutions in sterile H_2O were added into the wells (end concentrations 1, 2.5, 5, 10 μM) and the cells were again incubated for another 24 h. The plates were centrifuged (300 g, 5 min, 4 °C) and the supernatant was removed as described for the MTT assay. 50 μL of NBT in PBS (0.1%) was added into each well. After another 4 h of incubation at 37 °C the plates were centrifuged as before and the NBT solution was replaced with 50 μL of a 2 M KOH solution, and subsequently, 65 μL of DMSO was added into each well. After 30 min of incubation at 37 °C the absorbance of the formazan and the background was measured at 405 nm at 630 nm. Analogously, a second 96-well plate was prepared and an MTT assay was performed as described.

4.2.10. Caspase-3/-7 activation

The activation of caspases 3 and 7 was monitored using the Apo-One® Homogeneous Caspase-3/7 Assay (Promega), largely following the given protocol. 518A2 cells were seeded at 0.1×10^6 cpm into the wells of a 96-black well plate (67.5 μL/well) and the plate was incubated for 24 h under standard cell culture conditions. For each concentration, wells containing just DMEM without cells were prepared for background measurements. The cells were treated with **11a** (10 μM), **12a** and **13a** (each 5 μM), staurosporine (st) as a positive control (2 μM), and an analogous amount of the solvent as a negative control for 4 h at 37 °C. The provided substrate and buffer were prepared accordingly (1:100 dilution) and added to the wells (75 μL/well). After 2 h of incubation at room temperature in the dark, the fluorescence of the converted substrate was measured at 499 nm_{ex} / 527 nm_{em}. Analogously, a second plate for MTT assays was prepared and measured.

Declaration of Competing Interest

The authors declare that they have no known competing financial interests or personal relationships that could have appeared to influence the work reported in this paper.

Acknowledgement

R.S. thanks the Deutsche Forschungsgemeinschaft, Germany, for a grant (Scho 402/12-2).

Appendix A. Supplementary material

Experimental data of **2a**, **6a**, and **7a**; NMR spectra of **2–13**; UV-vis stability studies of **2–8**; Fluorescence staining of Golgi apparatus in 518A2 melanoma cells; SEC chromatogram and SDS-page of the expressed ASAH1; Michaelis Menten curve of Rbm14-12 at doi:xxxx. Supplementary data to this article can be found online at https://doi.org/10.1016/j.bioorg.2020.103703.

References

[1] J. Newton, L. Santiago, M. Maceyka, S. Spiegel, Revisiting the sphingolipid rheostat: Evolving concepts in cancer therapy, Exp. Cell Res. 333 (2015) 195–200.
[2] C. Mao, L.M. Obeid, Ceramidases: regulators of cellular responses mediated by ceramide, sphingosine, and sphingosine-1-phosphate, Biochim. Biophys. Acta 1781 (2008) 424–434.
[3] O. Cuvillier, G. Pirianov, B. Kleuser, P.G. Vanek, O.A. Coso, S. Gutkind, S. Spiegel, Suppression of ceramide-mediated programmed cell death by sphingosine-1-phosphate, Nature 381 (1996) 800–803.
[4] L.M. Obeid, C.M. Lindaric, L.A. Karolak, Y.A. Hannun, Programmed cell death induced by ceramide, Science 259 (1993) 1769–1771.
[5] S.A. Morad, M.C. Cabot, Ceramide-orchestrated signaling in cancer cells, Nat. Rev. Cancer 13 (2013) 51–65.
[6] P. Nussbaumer, Medicinal chemistry aspects of drug targets in sphingolipid metabolism, ChemMedChem 3 (2008) 543–551.
[7] H. Sawai, N. Domae, T. Okazaki, Current status and perspectives in ceramide-targeting molecular medicine, Curr. Pharm. Des. 11 (2005) 2479–2487.
[8] A. Huwiler, U. Zangemeister-Wittke, Targeting the conversion of ceramide to sphingosine 1-phosphate as a novel strategy for cancer therapy, Crit. Rev. Oncol. Hematol. 63 (2007) 150–159.
[9] K. Kagedal, M. Zhao, I. Svensson, U.T. Brunk, Sphingosine-induced apoptosis is dependent on lysosomal proteases, Biochem. J. 359 (2001) 335–343.
[10] O. Cuvillier, V.E. Nava, S.K. Murthy, L.C. Edsall, T. Levade, S. Milstien, S. Spiegel, Sphingosine generation, cytochrome c release, and activation of caspase-7 in doxorubicin-induced apoptosis of MCF7 breast adenocarcinoma cells, Cell Death Differ. 8 (2001) 162–171.
[11] C. García-Ruiz, A. Colell, M. Marí, A. Molares, J.C. Fernández-Checa, Direct effect of ceramide on the mitochondrial electron transport chain leads to generation of reactive oxygen species, J. Biol. Chem. 272 (1997) 11369–11377.
[12] R. Xu, J. Jin, W. Hu, W. Sun, J. Bielawski, Z. Szulc, T. Taha, L.M. Obeid, C. Mao, Golgi alkaline ceramidase regulates cell proliferation and survival by controlling levels of sphingosine and S1P, Faseb J. 20 (2006) 1813–1825.
[13] W. Hu, R. Xu, G. Zhang, J. Jin, Z.M. Szulc, J. Bielawski, Y.A. Hannun, L.M. Obeid, C. Mao, Golgi fragmentation is associated with ceramide-induced cellular effects, Mol. Biol. Cell. 16 (2005) 1555–1567.
[14] S.M. Mandala, Sphingosine-1-Phosphatases, Prostaglandins 64 (2001) 143–156.
[15] A.H. Futerman, Y.A. Hannun, The complex life of simple sphingolipids, EMBO Rep. 5 (2004) 777–782.
[16] C. Bedia, L. Chamacho, J.L. Abad, G. Fabriàs, T. Levade, A simple fluorogenic method for determination of acid ceramidase activity and diagnosis of Farber disease, J. Lipid Res. 51 (2010) 3542–3547.
[17] C. Voelkel-Johnson, J.S. Norris, S. White-Gilbertson, Interdiction of sphingolipid metabolism revisited; focus on protaste cancer, Adv. Cancer Res. 140 (2018) 265–293.
[18] M. Raisova, G. Goltz, M. Bektas, A. Bielawska, C. Riebeling, A.M. Hossini, J. Eberle, Y.A. Hannun, C.E. Orfanos, C.C. Geilen, Bcl-2 overexpression prevents apoptosis induced by ceramidase inhibitors in malignant melanoma and HaCaT keratinocytes, FEBS Lett. 516 (2002) 47–52.
[19] R.S. Seelan, C. Qian, A. Yokomizo, D.G. Bostwick, D.I. Smith, W. Liu, Human acid ceramidase overexpressed but not mutated in prostate cancer, Genes Chromosomes Cancer 29 (2000) 137–146.
[20] S.F. Tan, X. Liu, T.E. Fox, B.M. Barth, et al., Acid ceramidase is upregulated in AML and represents a novel therapeutic target, Oncotarget 7 (2016) 83208–83222.
[21] E.M. Saied, C. Arenz, Inhibitors of ceramidases, Chem. Phys. Lipids 197 (2016) 60–68.
[22] S. Grijalvo, C. Bedia, G. Triola, J. Casas, A. Llebaria, J. Teixidó, O. Rabal, T. Levade, A. Delgado, G. Fabriàs, Design, synthesis and activity as acid ceramidase inhibitors of 2-oxooctanoyl and N-oleoylethanolamine analogues, Chem. Phys. Lipids 144

(2006) 69–84.
[23] E. Houben, Y. Uchida, W.F. Nieuwenhuizen, K. De Paepe, T. Canhaecke, W.M. Holleran, Kinetic characteristics of acidic and alkaline ceramidase in human epidermis, Skin. Pharmacol. Physiol. 20 (2007) 187–194.
[24] A. Spinedi, S. Di Bartolomeo, M. Piacentini, N-Oleoylethanolamine inhibits glucosylation of natural ceramides in CHP-100 neuroepithelioma cells: possible implications for apoptosis, Biochem. Biophys. Res. Commun. 255 (1999) 456–459.
[25] C. Bedia, D. Canals, X. Matabosh, Y. Harrak, J. Casas, A. Llebaria, A. Delgado, G. Fabriás, Cytotoxicity and acid ceramidase inhibitory activity of 2-substituted aminoethanol amides, Chem. Phys. Lipids 156 (2008) 33–40.
[26] A. Bielawska, M.S. Greenber, D. Perry, S. Jayadev, J.A. Shayman, C. McKay, Y.A. Hannun, (1*S*,2*R*)-D-*erythro*-2-(*N*-Myristoylamino)-1-phenyl-1-propanol as an inhibitor of ceramidase, J. Biol. Chem. 271 (1996) 12646–12654.
[27] J.M. Draper, Z. Xia, R.A. Smith, Y. Zhuang, W. Wang, C.D. Smith, Discovery and evaluation of inhibitors of human ceramidase, Mol. Cancer. Ther. 10 (2011) 2052–2061.
[28] N. Realini, C. Solorzano, C. Pagliuca, D. Pizzirani, A. Armirotti, R. Luciani, M.P. Costi, T. Bandiera, D. Piomelli, Discovery of highly potent acid ceramidase inhibitors with in vitro tumor chemosensitizing activity, Sci. Rep. 3 (2013) 1035.
[29] (a) R. Schobert, S. Seibt, K. Mahal, A. Ahmad, B. Biersack, K. Effenberger-Neidnicht, S. Padhye, F.H. Sarkar, T. Mueller, Cancer selective metallocenedicarboxylates of the fungal cytotoxin illudin M, J. Med. Chem. 54 (2011) 6177–6182;
(b) G. Lohmann, E. Vasyutina, J. Bloehdorn, N. Reinart, J.I. Schneider, V. Babu, G. Knittel, G. Crispatzu, P. Mayer, C. Prinz, J.K. Muenzner, B. Biersack, D.G. Efremov, L. Chessa, C.D. Herling, S. Stilgenbauer, M. Hallek, R. Schobert, H.C. Reinhardt, B. Schumacher, M. Herling, Targeting transcription-coupled nucleotide excision repair overcomes resistance in chronic lymphocytic leukemia, Leukemia 31 (2017) 1177–1186;
(c) C. Spoerlein-Guettler, K. Mahal, R. Schobert, B. Biersack, Ferrocene and (arene) ruthenium(II) complexes of the natural anticancer naphthoquinone plumbagin with enhanced efficacy against resistant cancer cells and a genuine mode of action, J. Inorg. Biochem. 138 (2014) 64–72;
(d) A. Gmeiner, K. Effenberger-Neidnicht, M. Zoldakova, R. Schobert, A methyltitanocene complex of schisandrol A with high efficacy against multi-drug resistant cervix and breast carcinoma cells, Appl. Organometal. Chem. 25 (2011) 117–120.
[30] H. Azuma, S. Ijichi, M. Kataoka, A. Masuda, T. Izumi, T. Yoshimoto, T. Tachibana, Short-chain 3-ketoceramides, strong apoptosis inducers against human leukemia HL-60 cells, Bioorg. Med. Chem. 15 (2007) 2860–2867.
[31] H. Yang, L.S. Liebeskind, A concise and scaleable synthesis of high enantiopurity (–)-D-*erythro*-sphingosine using peptidyl thiol ester-boronic acid cross-coupling, Org. Lett. 9 (2007) 2993–2995.
[32] J. Sot, F.M. Goñi, A. Alonso, Molecular associations and surface-active properties of short- and long-N-acyl chain ceramides, Biochim Biophys. Acta 1711 (2005) 12–19.
[33] A. Dementiev, A. Joachimiak, H. Nguyen, A. Gorelik, K. Illes, S. Shabani, M. Gelsomino, E.E. Ahn, B. Nagar, N. Doan, Molecular Mechanism of Inhibition of Acid Ceramidase by Carmofur, J. Med. Chem. 62 (2019) 987–992.
[34] K. Bernardo, R. Hurwitz, T. Zenk, R.J. Desnick, K. Ferlinz, E.H. Schuchman, K. Sandhoff, Purification, characterization, and biosynthesis of human acid ceramidase, J. Bio. Chem. 270 (1995) 11098–11102.
[35] J.H. Park, E.H. Schuchman, Acid ceramidase and human disease, Biochim. Biophys. Acta. 1758 (2006) 2133–2138.
[36] J. Koch, S. Gartner, C.M. Li, L.E. Quintern, K. Bernardo, O. Levran, D. Schnabel, R.J. Desnick, E.H. Schuchman, K. Sandhoff, Molecular cloning and characterization of a full-length complementary DNA encoding human acid ceramidase, J. Biol. Chem. 271 (1996) 33110–33115.
[37] R. Huisgen, Centenary Lecture – 1,3-dipolar cycloadditions, Proc. Chem. Soc. (1961) 357–396.
[38] C.W. Tornøe, C. Christensen, M. Meldal, Peptidotriazoles on Solid Phase: [1,2,3]-triazoles by rediospecific copper(I)-catalyzed 1,3-dipolar cycloadditions of terminal alkynes to azides, J. Org. Chem. 67 (2002) 3057–3064.
[39] V.V. Rostovtsev, L.G. Green, V.V. Fokin, K.B. Sharpless, A stepwise Huisgen cycloaddition process: copper(I)-catalyzed regioselective ligation of azides and terminal alkynes, Angew. Chem. Int. Ed. Engl. 41 (2002) 2596–2599.
[40] K. Li, L.A. Lee, Q. Wang, Fluorogenic “click” reaction for labeling and detection of DNA in proliferating cells, Biotechniques 49 (2010) 525–527.
[41] K. Sivakumar, F. Cie, B.M. Cash, S. Long, H.N. Barnhill, Q. Wang, A fluorogenic 1,3-dipolar cycloaddition reaction of 3-azidocoumarins and acetylenes, Org. Lett. 6 (2004) 4603–4606.
[42] S. Bolte, F.P. Cordelieres, A guided tour into subcellular colocalization analysis in light microscopy, J. Microsc. 224 (2006) 213–232.
[43] https://imagej.nih.gov/ij/plugins/track/jacop.html.
[44] M.D. Abramoff, P.J. Magalhaes, S.J. Ram, Image processing with ImageJ, J. Biophotonics 11 (2004) 36–42.
[45] K. Indranil, M. Ratnava, J. Manoranjan, K.C. Shital, A stereodivergent route to four stereoisomeric 3́-acetoxycyclopentenylglycin derivatives, Synthesis 2 (2012) 304–310.
[46] A.J. Macuso, S.-L. Huang, D. Swern, Oxidation of long-chain and related alcohols to carbonyls by dimethyl sulfoxide “activated” by oxalyl chloride, J. Org. Chem. 43 (1978) 2480–2482.
[47] W. Oppolzer, R.N. Radinov, E. El-Sayed, Catalytic asymmetric synthesis of macrocyclic (*E*)-allylic alcohols from ω-alkynals via intramolecular 1-alkenylzinc/aldehyde additions, J. Org. Chem. 66 (2001) 4766–4770.
[48] S. Vanicek, H. Kopacka, K. Wurst, T. Müller, H. Schottenberger, B. Bildstein, Chemoselective, practical synthesis of cobaltocenium carboxylic acid hexafluorophosphate, Organometallics 33 (2014) 1152–1156.
[49] B.T. Loughrey, M.L. Williams, P.G. Parson, P.C. Healy, Nucleophilic substitution reactions of $[(\eta^5\text{-Cp}^*)\text{Ru}(\eta^6\text{-C}_6\text{H}_5\text{CO}_2\text{H})]^+$: synthesis, characterization and cytotoxicity of organoruthenium ester and amide complexes, J. Organomet. Chem. 819 (2016) 1–10.
[50] C. Bedia, J. Casas, V. Garcia, T. Levade, G. Fabriás, Synthesis of a novel ceramide analogue and its use in a high-throughput fluorogenic assay for ceramidases, ChemBioChem 8 (2007) 642–648.
[51] A. Gebai, A. Gorelik, Z. Liz, K. Illes, B. Nagar, Structural basis for the activation of acid ceramidase, Nat. Commun. 9 (2018) 1621–1632.